

The Coronal Physics Investigator (CPI) Experiment for ISS: A New Vision for Understanding Solar Wind Acceleration

J. L. Kohl,¹ S. R. Cranmer,¹ J. C. Raymond,¹ T. J. Norton,¹ P. J. Cucchiaro,² D. B. Reisenfeld,³
P. H. Janzen,³ B. D. G. Chandran,⁴ T. G. Forbes,⁴ P. A. Isenberg,⁴ A. V. Panasyuk,¹ and
A. A. van Ballegooijen¹

¹Harvard-Smithsonian CfA, ²L-3 Com IOS, ³U. Montana, ⁴U. New Hampshire

Abstract

In February 2011 we proposed a NASA Explorer Mission of Opportunity program to develop and operate a large-aperture ultraviolet coronagraph spectrometer called the Coronal Physics Investigator (CPI) as an attached International Space Station (ISS) payload. The primary goal of this program is to identify and characterize the physical processes that heat and accelerate the primary and secondary components of the fast and slow solar wind. In addition, CPI can make key measurements needed to understand CMEs. CPI is dedicated to high spectral resolution measurements of the off-limb extended corona with far better stray light suppression than can be achieved by a conventional instrument.

UVCS/SOHO allowed us to identify what additional measurements need to be made to answer the fundamental questions about how solar wind streams are produced, and CPI's next-generation capabilities were designed specifically to make those measurements. Compared to previous instruments, CPI provides unprecedented sensitivity, a wavelength range extending from 25.7 to 126 nm, higher temporal resolution, and the capability to measure line profiles of He II, N V, Ne VII, Ne VIII, Si VIII, S IX, Ar VIII, Ca IX, and Fe X, never before seen in coronal holes above 1.3 solar radii. CPI will constrain the properties and effects of coronal MHD waves by (1) observing many ions over a large range of charge and mass, (2) providing simultaneous measurements of proton and electron temperatures to probe turbulent dissipation mechanisms, and (3) measuring amplitudes of low-frequency compressive fluctuations.

CPI is an internally occulted ultraviolet coronagraph that provides the required high sensitivity without the need for a deployable boom, and with all technically mature hardware including an ICCD detector. A highly experienced Explorer and ISS contractor, L-3 Com Integrated Optical Systems and Com Systems East, will provide the tracking and pointing system as well as the instrument, and the integration to the ISS.

1. Background and Motivation

This white paper summarizes the proposed Coronal Physics Investigator (CPI) experiment. It is being circulated together with a poster presentation to be given by Raymond et al. at the June 12–16, 2011 meeting of the Solar Physics Division of the AAS in Las Cruces, New Mexico.

CPI (pictured in Figure 1) follows on from the discoveries of UVCS/SOHO to answer the basic question: *What physical processes heat and accelerate both the major (proton, electron, helium) and minor (heavy ion) plasma components of the fast and slow solar wind?* In the remainder of this section, we outline the historical context of CPI and how this experiment will fundamentally transform our observational understanding of solar wind acceleration. Section 2 gives additional information about the scientific goals of CPI. Section 3 describes the CPI science payload, and Section 4 discusses the accommodation of CPI on the ISS. Section 5 gives an overview of the CPI mission, and Section 6 describes the CPI team, management, and costs.

Ultraviolet spectroscopy of the extended solar corona (defined here as ≥ 1.4 solar radii, R_{\odot} , from Sun center) has become a powerful tool for obtaining detailed empirical descriptions of the regions where solar wind streams and coronal mass ejections (CMEs) undergo most of their acceleration. Ultraviolet spectroscopy allows us to determine the velocity distributions and outflow velocities of protons and minor

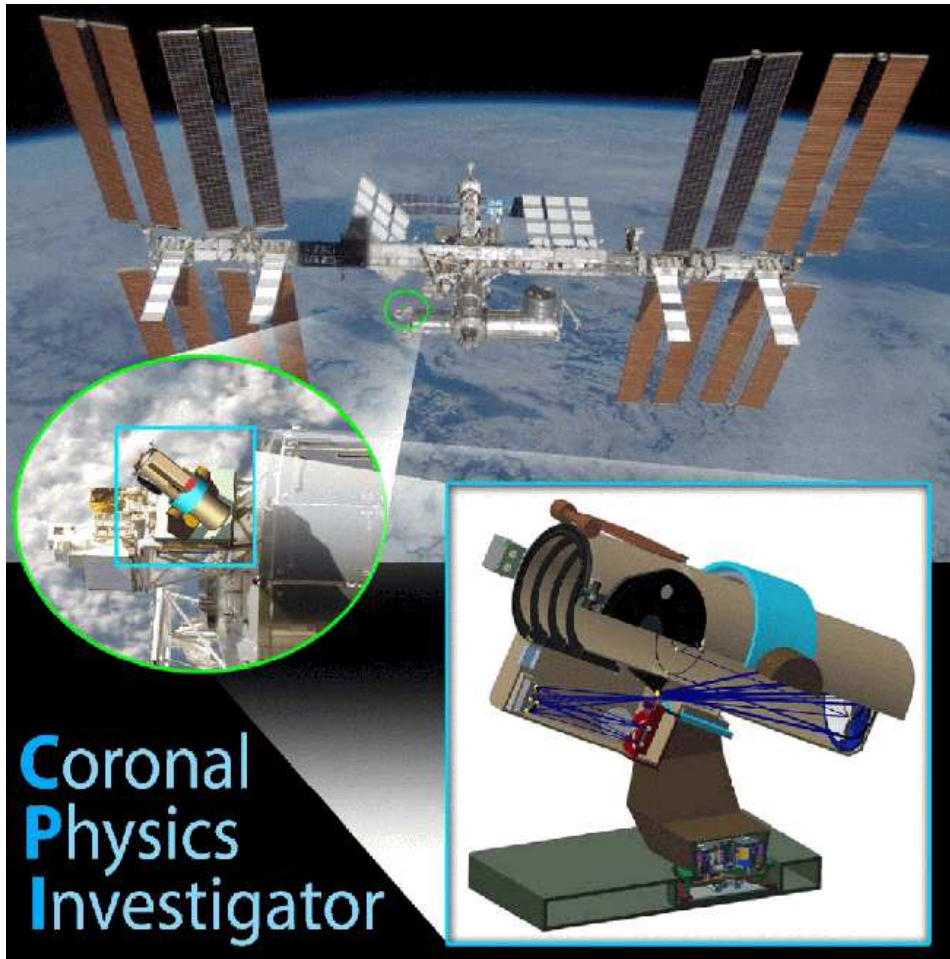


Figure 1: CPI has been proposed as a Small Complete Mission for the International Space Station (ISS). The baseline location for CPI on ISS is the Columbus EPF Starboard Overhead Zenith (SOZ) site.

ions near the Sun, it provides absolute chemical abundances and charge state distributions, and it is capable of determining the velocity distributions and densities of electrons (e.g., Withbroe et al. 1982; Kohl et al. 2006). These observations provide the constraints needed to test and guide theoretical models of extended coronal heating, solar wind acceleration, and CME production.

Occluded ultraviolet telescope-spectrometers were first developed and flown on sounding rockets (1979, 1980, 1982) and on the Shuttle-deployed *Spartan 201* payload (1993, 1994, 1995, 1998); see, e.g., Kohl et al. (1978, 1994, 2006). Following on the successes of these pilot observations, the Ultraviolet Coronagraph Spectrometer (UVCS) instrument was flown on the ESA/NASA *Solar and Heliospheric Observatory (SOHO)* spacecraft (Kohl et al. 1995). UVCS/SOHO began observing in 1996 and is scheduled to continue operations until September 2012.

In the fast solar wind, UVCS discovered remarkably strong preferential ion heating for O^{+5} and Mg^{+9} and pronounced kinetic anisotropies (with $T_{\perp} > T_{\parallel}$) in polar coronal holes (Kohl et al. 1997, 1998, 2006; Cranmer et al. 1999, 2008). These results rekindled theoretical efforts to understand the heating of the extended corona by ion cyclotron resonance (Hollweg & Isenberg 2002), though we still do not understand how these waves are produced. In the slow solar wind, much of which originates in streamers, efforts have centered on attempts to understand the relative roles of reconnection and magnetic flux tube geometry, but there is evidence for wave processes similar to those seen in the fast wind (Frazin et al. 2003).

Despite the advances outlined above, though, the diagnostic capabilities of UVCS were limited to what was foreseen before *SOHO* (when only H I Ly α had been observed). UVCS allowed us to identify what additional measurements need to be made to answer the fundamental questions about how solar wind streams are produced, and we have designed the next-generation capabilities of the CPI experiment specifically to make those measurements. As will be described below in more detail, CPI provides unprecedented sensitivity, a wavelength range extending from 25.7 to 126 nm, improved time resolution, and the capability to measure UV line profiles never before seen in coronal holes in the extended corona. CPI would be the first mission to be able to fully characterize the plasma properties in the region where the solar wind's primary energy and momentum addition occurs.

The CPI coronagraph spectrometer design is a departure from earlier next-generation concepts that achieved the required increase in sensitivity with a remote external occulter mounted on a deployable boom, and improved detector performance with an Intensified Active Pixel Sensor (IAPS) detection system with a high maximum count per pixel capability. CPI achieves its high sensitivity with an internally occulted coronagraph design that provides up to a factor of 200 increase in count rates over UVCS/*SOHO*. Since solar disk to solar coronal intensity ratios in the ultraviolet are smaller than for visible light, it was possible to design the internally occulted CPI to have sufficient stray light suppression to observe spectral lines of interest in coronal holes at the crucial heights of $> 1.8 R_{\odot}$, where collisionless wave-particle interactions are believed to dominate. CPI uses an ICCD detector similar to those provided for *Swift* and *XMM/Newton* by the Mullard Space Science Laboratory. This detector meets all of the CPI observation requirements, and eliminates any question about its technical readiness level. The CPI resource requirements are well within the capabilities of the ISS, which can provide 16 orbits per day and 310 days per year of solar observations. By taking advantage of the existing capabilities of ISS, CPI achieves its science goals at far less cost than would be needed for an independent mission.

The CPI project will not only make a tremendous advance in solar wind science, it will provide a bridge to the next solar maximum when there is considerable interest in a mission to focus on the most energetic flares, CMEs, and energetic particle acceleration events (e.g., the *SEE 2020* mission concept; Lin et al. 2010). The new CPI team—including Dan Reisenfeld as Project Scientist and Paul Janzen as Instrument Scientist, as well as Tim Norton as Project Manager and the new collaboration with the industrial partner L-3 Com Integrated Optical Systems—would continue to be in place for this opportunity.

CPI fits well into the constraints of an Explorer Small Complete Mission with large technical reserves, seven months of costed schedule reserves beyond a robust 48 month phase B/C/D baseline development schedule, 25% cost reserves plus a 5% margin, and a \$4M descope plan with vary little impact on the primary science.

2. Scientific Goals and Objectives

2.1. Solar Wind Acceleration

CPI will address the fundamental question of the identification of the energy and momentum deposition processes that accelerate the solar wind. Figure 2 illustrates the range of solar wind issues to be explored by CPI. A large body of space-based and ground-based observations suggests that Alfvén waves exist in the lower solar atmosphere and carry enough power to accelerate the wind and heat the quiet corona (e.g., Cranmer & van Ballegoijen 2005; De Pontieu et al. 2007; Moore et al. 2011). However, the mechanisms that convert these waves into heat and kinetic energy are still not understood. The lack of tight constraints on the plasma properties near the Sun is the major roadblock to a comprehensive understanding of the relevant processes. Thus, CPI has been designed to make major breakthroughs by answering specific questions such as the following.

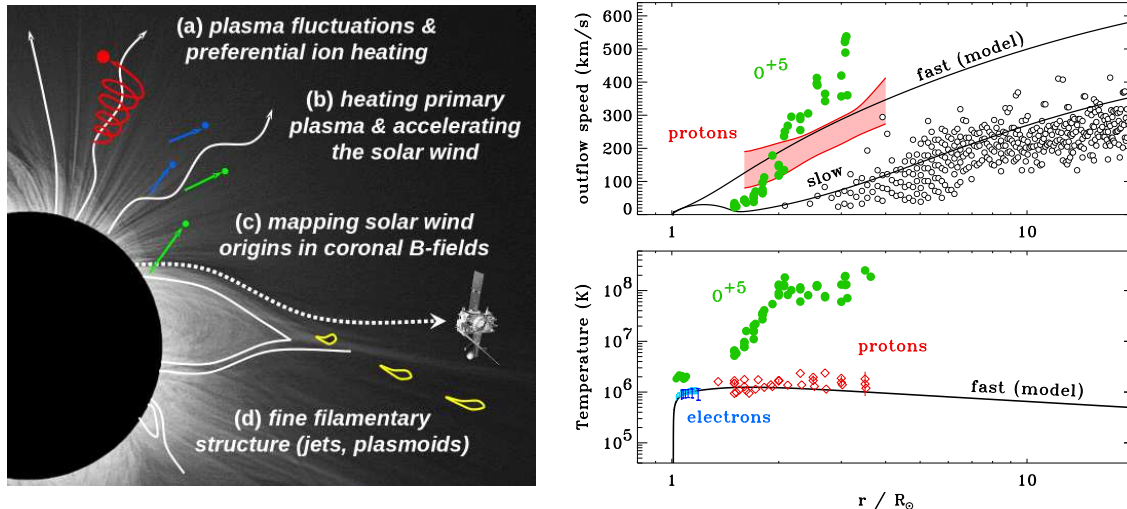


Figure 2: *Left:* Eclipse image (Pasachoff et al. 2007) overlaid with the solar wind questions addressed by CPI. *Right:* collection of coronal outflow speeds (top) and temperatures (bottom) from models and UV spectroscopy and coronagraph measurements. Black curves are model results from Cranmer et al. (2007). UVCS/SOHO measurements in coronal holes (red: protons, green: O^{+5}) are described in more detail by Cranmer (2009). Black open circles denote slow wind outflow speeds from Sheeley et al. (1997) and blue symbols denote electron temperatures from Wilhelm (2006) and Landi (2008).

How and where do plasma fluctuations drive the preferential ion heating and acceleration? UVCS discovered extreme ion properties in coronal holes that pointed to the damping of high-frequency (10 – 10^4 Hz) ion cyclotron waves, but these measurements were limited to only two minor ions (Kohl et al. 1998, 1999). Thus, it has been difficult to unambiguously confirm the ion cyclotron idea or distinguish it clearly from other processes such as stochastic Alfvén wave damping (e.g., Voitenko & Goossens 2004; Chandran 2010), shock acceleration (Lee & Wu 2000), or shear-driven instabilities (Markovskii et al. 2006). By measuring the properties of ions with a wide range of charge and mass over a large range of heights, CPI will tightly constrain the properties of the spectrum of fluctuations thanks to its high sensitivity and large spectral coverage. By comparing CPI minor ion measurements to the predictions of kinetic and MHD models, we can tightly constrain the spectral slope, the local damping, and the precise modes (Alfvén, fast, slow) of the waves. As the number of ions observed in each region increases, our confidence in the uniqueness of a successful theoretical model (based on a given process) increases as well.

What processes contribute to heating the primary (proton, electron, helium) plasma in the extended corona and accelerating the solar wind? CPI will determine the degree of bulk-plasma heating and acceleration from the most likely physical processes. The properties of the resonant wave spectrum (from the previous question) are key inputs to this question as well, but additional CPI observations are needed to constrain the full range of processes. The primary UV measurements for this question are the proton, electron, and helium plasma properties; e.g., H I Ly α resonance scattering line profiles (H^0 is closely coupled to protons by charge transfer; Allen et al. 2000), H I Ly α Thomson scattering line profiles (a probe of the electron velocity distribution), and He II 30.4 nm line profiles. The methodology for this question involves comparing heating and acceleration rates (derived from measured temperatures, densities, and outflow speeds) to rates predicted by theoretical models of the following:

1. **High-frequency (or other ion-resonant kinetic) waves:** The information about the resonant wave spectrum obtained from minor ions can be extrapolated to predict proton and helium energization rates that are associated with the specific “flavor” of wave-particle interaction that is evaluated to be consistent with the ion measurements discussed above.

2. **Low-frequency waves:** CPI can constrain the amplitudes of low-frequency waves that may not be efficient at heating minor ions. These waves can accelerate the plasma by wave pressure and possibly heat electrons via Landau damping. Preliminary observations of long-period (10–20 minute) compressive fluctuations in coronal holes have been made (e.g., DeForest & Gurman 1998; Krishna Prasad et al. 2011), but CPI can confirm and better characterize the full plasma response to these fluctuations. Also, models that predict significant ponderomotive acceleration from low-frequency waves (Ofman & Davila 2001) can be tested by constraining the available power.
3. **Suprathermal particles:** Ubiquitous in space plasmas, particles in the tails of proton and electron velocity distributions have been suggested as key contributors to coronal heating (Scudder 1992; Viñas et al. 2000) and in determining *in situ* charge states (Esser & Edgar 2000). The presence of strong tails in the very low corona is doubtful because of the high collision rate (Feldman et al. 2007), but CPI can detect these tails in proton and electron distributions (via departures from Gaussian shapes in the H I Ly α profiles) well into the collisionless domain at large heights.

CPI will also answer detailed questions about mapping the origins of *in situ* solar wind streams down to the coronal magnetic field, and about the role of episodic jets and reconnection in the solar wind’s mass and energy budget. These questions are discussed further in Section 2.3 below, along with the contributions of other NASA heliophysics missions. In addition, the improved understanding of coronal physics that CPI will facilitate is important not only for explaining the origins of space weather, but also for establishing a baseline of knowledge directly relevant to other stars and astrophysical systems ranging from the interstellar medium to black hole accretion disks.

2.2. Coronal Mass Ejections (CMEs)

CMEs are a secondary objective for CPI because solar minimum conditions will prevail during the mission’s primary phase. Nevertheless, there will be one CME every 2–3 days based on LASCO observations (Yashiro et al. 2004), and we expect to observe 30 to 50 CMEs during the primary mission and considerably more during the extended mission thanks to increasing solar activity. UVCS demonstrated the power of spectroscopy to unravel the physics of CMEs (see Kohl et al. 2006), but new observational capabilities are needed to answer the most fundamental questions. CPI will provide a wide range of unambiguous diagnostics for the physical conditions of CMEs. This is enabled by a multi-slit capability and the sensitivity and spectral range that permit observation of He II 30.4 nm and several density-diagnostic line ratios (e.g., Ne VII 89.5/88.7 nm and O VI 55.4/55.5 nm) to constrain time-dependent ionization models of the expanding plasma. CPI will address the following questions.

What physical processes drive the evolution and heating of CMEs in the corona? UVCS data have been used to reconstruct the 3D structures and thermal histories of a small number of CMEs, and there is evidence that the plasma in CMEs is strongly heated as it accelerates (e.g., Lee et al. 2009; Landi et al. 2010). The nature of the heating is not known, but a number of energization mechanisms have been proposed (Kumar & Rust 1996; Lin et al. 2004; Reeves et al. 2010; Murphy et al. 2011). CPI will help distinguish between the predictions of these different models by measuring plasma parameters not only in the brightest parts of CMEs (e.g., the bright front and the twisted remnants of the prominence or flux rope) but also in the dimmer “void” region behind the front and the shock ahead of the front.

What is the role of magnetic reconnection in the eruption and relaxation of the coronal magnetic field in CMEs? In the classic CME picture (Sturrock & Coppi 1966), an erupting flux rope leaves behind oppositely directed open fields that are separated by a current sheet. Reconnection in this sheet produces an arcade of post-CME loops seen as large X-ray flares, at the same time allowing the twisted flux rope to escape as the CME plasmoid (Lin & Forbes 2000). In a few events, UVCS detected spatially narrow emission features in [Fe XVIII] 97.4 nm (formed at $T_e \approx 6$ MK) that match the expected properties of thin current sheets

(Raymond 2008). CPI will observe many more lines from the extremely hot plasma at these reconnection sites, up to [Fe XXII] 82.2 nm, with improved sensitivity. Line ratios will be used to infer the electron temperature, density, and flow speeds (Ko et al. 2010). Line widths measured by CPI can be used to put limits on the velocity amplitude of turbulent motions in current sheets (see Kowal et al. 2009).

2.3. Relationships to Other NASA Missions

A unique strength of CPI is how it both strongly complements and is complemented by other NASA solar missions planned for the same time period. The following questions represent examples of the wider science objectives achievable by integrating CPI measurements with those from other missions.

How do nanoflares and magnetic reconnection affect the solar wind? UV and X-ray imaging instruments on *SDO*, *Hinode*, *STEREO*, *IRIS*, and *Solar Orbiter* will put tight new constraints on the mechanisms responsible for the intermittent energy release from reconnection events below $\sim 1.2 R_{\odot}$. CPI measurements above $1.4 R_{\odot}$ provide the radial dependence of the heating rates and constrain the parameters of reconnection-based solar wind models (Fisk 2003; Antiochos et al. 2011). CPI will also have the sensitivity to identify rapid thermal changes associated with the postulated field-line motions in jet-like reconnection events that are detected closer to the disk with instruments like *AIA/SDO* and *IRIS* (e.g., Yang et al. 2011).

How do plasma properties and magnetic field lines connect from the photosphere to the heliosphere? A key goal of space weather prediction is the ability to map magnetic field from the Sun to 1 AU. Currently this is done by using disk images and magnetograms (e.g., *MDI/SOHO* and *HMI/SDO*) as lower boundary conditions and *in situ* particle and field data to test the results of MHD models. CPI makes possible a more complete picture of this 3D system by providing the “missing link” between data at $1 R_{\odot}$ and 1 AU. It also aids in the interpretation of inner heliospheric measurements by *Solar Probe Plus* and *Solar Orbiter* by probing the plasma properties in the wind’s acceleration region. The stable coronal structure at solar minimum will permit tomographic reconstruction of these plasma properties (Panasyuk et al. 1999; Frazin et al. 2009; van der Holst et al. 2010), so that global MHD models can be better tested and refined. CPI also provides elemental abundance and charge state data for minor ions, which is another way to trace the origin of *in situ* solar wind streams (e.g., Ko et al. 2006; Zurbuchen 2007). CPI will build up an unprecedented database of abundance maps that will test models of fractionation and the First Ionization Potential (FIP) effect from gravitational settling (Lenz 2004) and MHD waves (Laming 2009).

3. The CPI Science Payload

3.1. Instrumentation Overview

The CPI Science Payload (SP) is comprised of the Coronagraph-Spectrometer Unit (CSU), the Gimbals Pointing Unit (GPU), and the Remote Electronics Unit (REU); see Figure 3. The CSU is further comprised of the Telescope Assembly (TA) and the Spectrometer Assembly (SPA). The TA feeds light to the SPA, which consists of a toric dual-grating spectrometer with an intensified CCD (ICCD) detection system. The SP has two optical paths: the EUV path (EUVP) for spectroscopy at 68.0–126 nm, and the He II path (HeP) for spectroscopy at 49.5–84 nm (1st order) and 25.7–42.0 nm (2nd order). It obtains high resolution spectra of spatial regions as small as $4.5''$. The field of view is shown in Figure 4.

A key capability of CPI is that it facilitates determination and removal of the stray light spectrum for each observed height with solar disk observations scaled with the intensities of isolated stray light spectral features observed during coronal measurements.

The CSU optical layout is shown in Figure 5. Light enters through the 16.8 cm diameter Entrance Aperture (EA) and falls on the Telescope Mirror (TM), which is under-filled for both the solar disk and

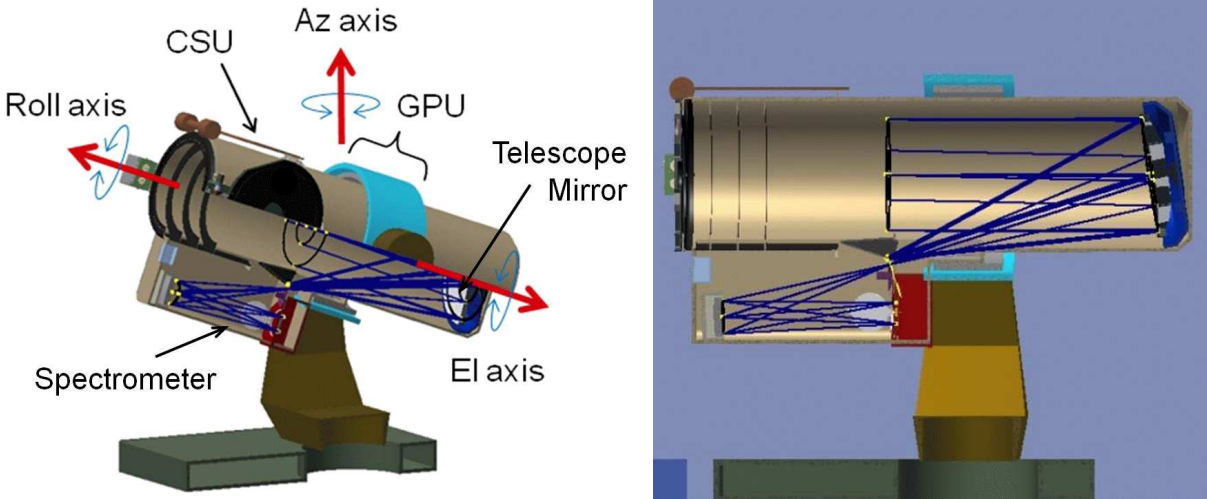


Figure 3: CPI in its on-orbit (left) and transport (right) configurations.

coronal radiation. One half of the mirror surface is SiC for illumination of the EUV path and the other half is coated with Si/Mo-Ir for the He II path. For coronal observations, the GPU and TM place an image of the disk on the Solar Disk Light Trap, which is elongated in the radial direction to allow coronal images at heights of 1.4 to 3.5 R_{\odot} to be centered on the SPA Entrance Slit. This light trap is similar to that of UVCS/*Spartan* (Kohl et al. 1994, 2006) and consists of a polished high-reflectance mirror at an oblique angle that reflects the direct solar disk radiation into a blackened cavity with close-packed 5 mm diameter tubes. The mirror forms a 1.7 times magnified image of the EA at 136 cm, which is beyond the SPA Entrance Slit and Gratings. Most of this light is intercepted by the slit jaws, and the portion that passes through the slit is intercepted by a light trap that is located just in front of the gratings and surrounds them. There are baffles between the entrance aperture and telescope mirror, and all non-optical surfaces in the telescope are designed to attenuate stray light. There is no CPI hardware Sunward of the EA.

The Toric Dual-Grating Spectrometer has an Entrance Slit mechanism with 5 selectable slits of varying widths and a set of three slits for simultaneous observations at multiple heights. Coronal light passes through the slit and onto two toric gratings, one for each light path. The gratings act nearly as one optic. The grating size is chosen to not accept any light that contributes to the image of the Entrance Aperture including diffraction of that light by the slit, as well as to not accept light from the outer portion of the mirror that would have unacceptable imaging properties. The gratings are slightly tilted with respect to one another in the perpendicular to dispersion direction, so that their focal planes are offset by 2.0 mm at the detector. They are oriented in the dispersion direction to minimize overlap between the coronal lines of the two paths. There is a grating drive that is used to optimize image/spectral quality for spectral lines near the outer limits of the EUV wavelength range, and also to facilitate avoidance of any detector imperfections. The pivot axis is 4.09 cm from the center of the grating surface. The SPA has light traps for zero order and for intercepting light from the Entrance Aperture edges as well as a baffle located between the gratings and the detector to ensure that the detector only views rays from the gratings.

Optical performance of CPI was modeled with ZEMAX and is illustrated for the EUV path in Figure 6. The HeP performance also meets all of the requirements. CPI provides a tremendous improvement in count rates over UVCS/*SOHO* for the portion of the CPI wavelength range covered by UVCS (e.g., factors of 200, 40, and 20 at 1.4, 1.8, and 2.5 R_{\odot} , respectively for observations of O VI 103.2 nm). This is the result of a greatly increased unvignetted telescope area and improved reflective coatings and detector counting efficiency.

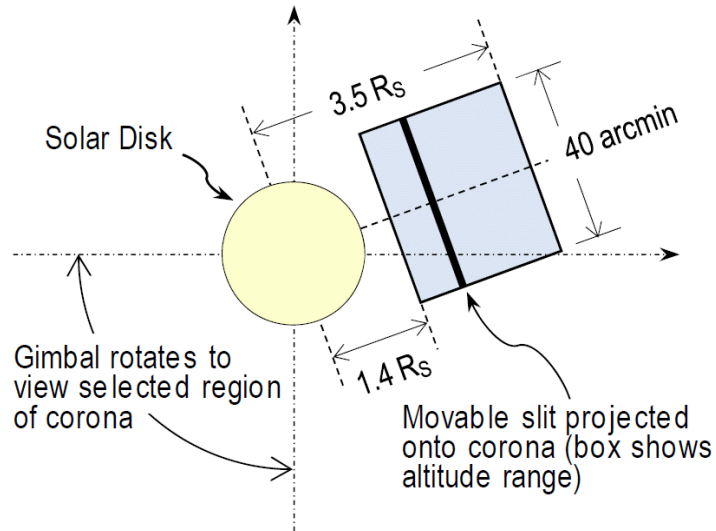


Figure 4: The CPI field of view (FOV).

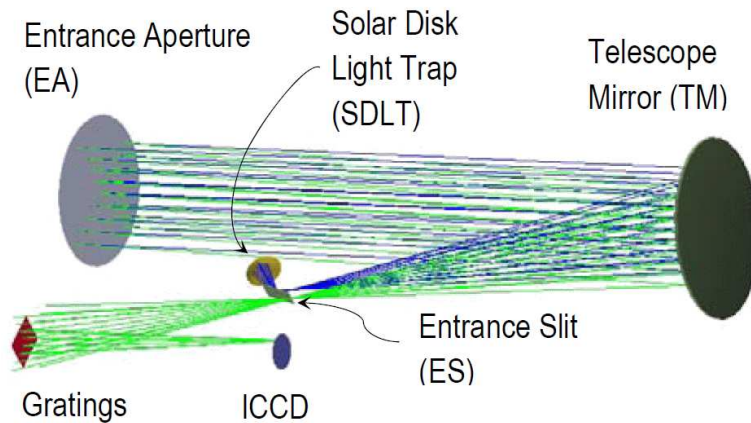


Figure 5: ZEMAX rendering of CPI optical layout. Shown are coronal rays (green) from an altitude of $3.5 R_{\odot}$ that pass into the spectrometer, while disk light (blue) is redirected into the Solar Disk Light Trap. Rays that miss the grating include all rays from the EA.

3.2. Stray Light Suppression

Stray light suppression is sufficient for all required observations (see Figure 7). The fundamental and dominant source of stray light is due to diffraction by the finite size of the entrance aperture and telescope mirror. To minimize this diffraction, the entrance aperture and mirror are oversized so that the focal ratio is much smaller ($f/2.5$) than the focal ratio of the gratings (effective focal ratio of $f/7$). In this way, the diffracted light from the mirror that passes through the SPA slit and onto the gratings can be reduced approximately in proportion to the diameter of the entrance aperture. Other sources of stray light are made negligible with careful design. Direct solar-disk light is specularly reflected off the telescope mirror and imaged onto the Solar Disk Light Trap, which reduces it to negligible levels. Solar disk radiation that encounters particulate contamination on the reflecting surface of the telescope primary has been shown to be controllable to negligible levels. Scattering due to mirror figure errors and microroughness are reduced to near negligible levels. Observational lines of sight are restricted such that glints off surfaces of the ISS illuminate the EA at large ($> 10^{\circ}$) angles. This prevents any glint light from falling on the portion of the telescope mirror that has straight-line or slit-diffracted paths to the gratings. Baffles on the TA

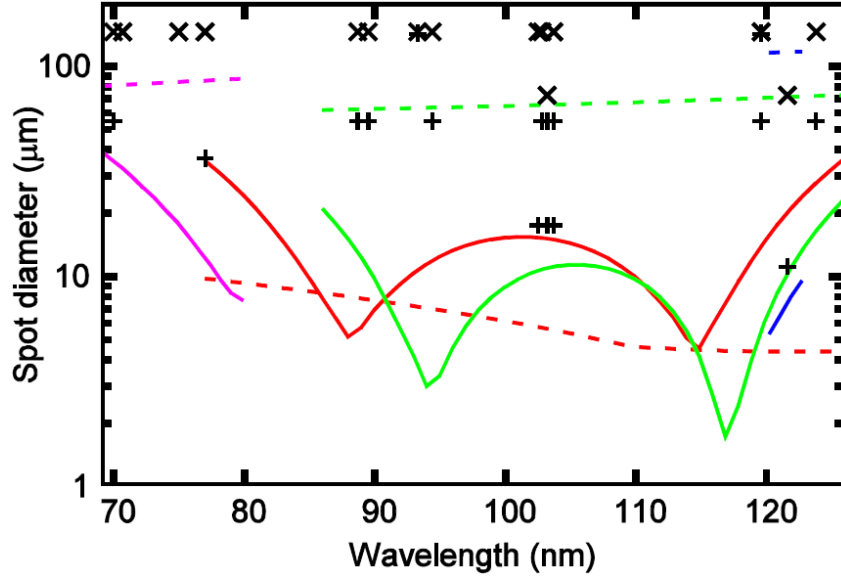


Figure 6: Predicted spectral (solid lines) and spatial (dashed lines) FWHM spot diameters of the EUV channel. Grating positions for four observation modes are shown: standard (red), jet observations (green), H I Ly α (blue), and short wavelength (pink). Points represent spectral (+) and spatial (x) requirements.

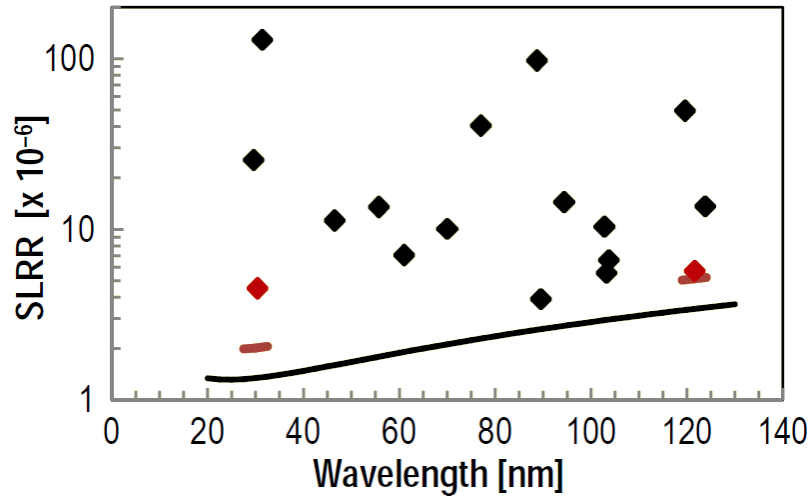


Figure 7: Stray light reduction ratios. Lines indicate modeled CPI stray light levels at $1.8 R_{\odot}$ (red: He II 30.4 nm, H I Ly α) and $2.0 R_{\odot}$ (black: all other lines). Corresponding colored points show stray light requirement for coronal hole spectral lines.

structure effectively eliminate glints that enter the EA at angles that miss the mirror. It is also necessary to reduce the solar disk light at wavelengths outside the band pass of the spectrometer. This off-band radiation is eliminated by the diffraction gratings for wavelengths shortward of 180 nm. Suppression at longer wavelengths, where the solar disk intensity is extremely high, is provided by a combination of the occulting system, the diffraction grating, and the low sensitivity of the ICCD detector.

Stray light characterization and removal will be accomplished with a combination of a stray light model together with laboratory stray light characterization, and during the mission, observations of the solar disk spectrum and direct detection of spectral features known to be due solely to stray light. The model will be refined during the instrument development. At this time, the stray light levels have been computed with a

series of empirically validated models that verified that the dominant contributor is finite-aperture diffraction from the entrance aperture. The other possible sources of stray light were found to be controllable and can be made negligible. A simple parameterized model of non-specular stray light was used to predict the expected stray light levels. The results of this analysis are provided in Figure 7. This model, which was validated by adapting it to the geometry and optical properties of UVCS/*SOHO*, predicts a level of stray light that agrees with in-flight measurements (see Cranmer et al. 2010). The model was used to determine preliminary microroughness and figure error specifications for the TM.

Modeling indicates that for most spectral lines of interest, the ratio of the coronal signal to the stray light will be sufficient to achieve the science goals with a minimum background analysis. However, for some important lines, CPI will be required to accept and remove stray light levels that are comparatively high; for example, reaching an estimated level of 1:1.5 corona-to-stray light ratio at $1.8 R_{\odot}$ for H I Ly α and He II 30.4 nm in coronal holes.

The characterization and removal of the stray light background will use a combination of the synchronous solar disk observations (with a reduced aperture to bring the count rate within the dynamic range of the ICCD detector), the measurements of spectral features produced solely by stray light, and coronal hole observations above $2.5 R_{\odot}$, which will be almost entirely stray light in the case of H I Ly α and He II 30.4 nm. Laboratory stray light calibration data will be used to extrapolate stray light contributions to lower altitudes, and to determine the stray light level as a function of the origin of the light on the disk and the observed height above the solar limb in order to verify parameters in the stray light model, which in turn will be used with in-flight solar disk observations to weight the stray light contributions from various parts of the disk. All observations will be modeled as a combination of coronal emission, stray light, and detector background. In addition, H I Ly α observations will include a model of geocoronal emission and absorption. All the components except coronal emission have well known or separately measurable spectral shapes. The relative contributions of the components will be varied to achieve the best fit to the observed data, but the range of their variation will be highly constrained by the laboratory stray light model, the measured stray light spectral features, and the solar disk spectrum (as well as, in the case of H I Ly α , a geocoronal model similar to the one used for the UVCS/*Spartan* (Kohl et al. 1996).

Coronal emission will be modeled as a combination of a Gaussian core and high-velocity wings, corresponding to electron scattering and possibly suprathermal particle scattering. The characteristic spectral widths of the coronal emission components are significantly higher than the rest of the contributing features, which facilitates high-precision component separation. In summary, because (1) a high quality advance knowledge of the stray light characterization will exist, (2) measurements of the stray light will exist at nearby wavelengths, and (3) very recent measurements of the solar disk spectrum with the same instruments will exist, then model fitting with a very limited number of highly constrained “free parameters” will result in the stray light removal procedure being extremely robust. The precision of the coronal profile recovery is expected to be at the level of 5% or better, even for signal to stray light ratios of greater than 1:1.5.

3.3. ICCD Detector

The detector consists of a 40 mm diameter microchannel plate (MCP) intensifier with a fiber optic output window optically coupled to a CCD. The MCP is coated with KBr. The intensifier includes a vacuum door and non-flight 2 liter/s ion pump. This detector has a high technical reliability since it is essentially the same technology that the Mullard Space Science Laboratory (MSSL) used for the ICCD detectors on *Swift* (Roming et al. 2000) and *XMM/Newton* (Mason et al. 2001). Following assembly, the detector is maintained under vacuum to prevent deterioration of the photocathode. A grid/aperture in front of the MCP repels low energy ions. The grid is set to ~ 100 V, and is adjustable in flight.

Individual photoelectrons are produced at the MCP surface and multiplied through its pores. Exiting electrons are accelerated onto a phosphor screen coupled to a CCD chip using a 3.5:1 fiber optic taper. Each

photoelectron results in a “splash” of light on a 3 pixel area of the CCD. The light splash is centroided to 0.25 pixels (spectral only), improving the resolution. A 1024×256 window is read out, allowing an increased frame rate.

If two events land in the same 3×3 pixel area during an exposure, the two events can be identified using a combination of pulse height and position information, and are both rejected from the image (although retained in a count register). To minimize this effect, the CCD is clocked at the maximum frame rate. The maximum acceptable count rate for CPI of 5.6 counts/s at a 50% loss rate is somewhat increased by two factors:

- a. The position resolution required in the spatial dimension is less critical than in the spectral dimension. This gives some relaxation in the proximity of events in that axis, where centroiding is not required.
- b. The maximum count rates are at the peaks of spectral lines. The shoulders and base of the lines are within 3 CCD pixels, so that the average count rate over 3 pixels is lower than at the peak. This effect allows a higher maximum count rate for the disk observations compared to the coronal observations: lines on the disk are narrower, and so a higher peak count rate can be tolerated because the adjacent areas within the 3-CCD-pixel width have a lower rate.

3.4. Line of Sight Pointing System (LOSPS)

The tracking and pointing of the CPI Coronagraph Spectrometer Unit is provided by the Gimbals Pointing Unit (GPU) and a Telescope Mirror Pointing Subassembly (MPS). The GPU provides the coarse tracking of the Sun across the sky during orbital day, and the fine pointing of the instrument so that the solar disk image falls on the Solar Disk Light Trap and the coronal region of interest falls on the spectrometer entrance slit. The CSU is mounted in a Roll Axis Assembly that provides rotation of the CPI field of view about the Sun-center axis to place the image of the selected position angle axis on the center of the spectrometer slit. The Roll Axis Assembly is mounted in a yoke that provides rotation in the elevation axis, and the yoke is mounted on an Azimuth Assembly that provides rotation about the axis that is perpendicular to the elevation axis. Low frequency disturbances are removed by the GPU. Higher frequency vibrations over the small amplitudes expected on ISS are compensated with motions of the telescope mirror provided by the MPS. L-3 Com Integrated Optical Systems is highly experienced in such systems, having developed similar ones for the *WISE*, *HIRDLS*, *GIFTS*, and *GOES-R ABI* missions.

4. Science Payload Accommodation on ISS

ISS engineers at JSC have provided a preliminary confirmation that the CPI accommodation requirements are compatible with the ISS.

4.1. ISS External Research Accommodation Sites Characteristics

The primary ISS site for CPI is the Columbus Starboard Overhead Zenith (SOZ) site. This is the Columbus External Payload Facility zenith position which has been used for the Columbus SOLAR payload. The CPI accommodation requirements are well within the allowable SP mass, power, SP volume, and telemetry rates specifications for this site. Mounting, power, and data interfaces are standardized on pallet plates that ease mounting, robotic handling, and installation (e.g., the Columbus standard cargo interface called the Flight Releasable Attachment Mechanism; FRAM). After installation, the ISS provides data up/downlink and command and control via a standard interface at MSFC. At the end of the instrument’s lifetime, an established ISS procedure removes the payload and transports it for safe discard.

4.2. CPI ISS Resource Requirements

ISS capability provides a 54% reserve in addition to the CPI requirement for mass and 376% for power. CPI fits in the Columbus SOZ site and transport volume with ample reserves. The CPI data rate and data capacity requirements are less than 2% of the ISS capable data rate for both S and K band transmitter systems. Thermal ISS interfaces are capable of supporting CPI requirements. ISS contamination experts have informed us that the ISS is compatible with the CPI particulate and molecular contamination requirements as long as CPI follows its plan to never point at an ISS structure and to always close its Entrance Aperture Door during high contamination periods, which occur less than a few percent of the time.

4.3. ISS Orbit and Trajectories

The ISS ram direction is the x axis, the zenith is the z axis, and the orthogonal axis is y . The current ISS altitude varies from 350 to 460 km and is expected to increase to an average of 450 km prior to CPI operations. Atmospheric absorption will allow scientific observations to commence before the Sun vector reaches the xy plane. After consultation with the ISS MAGIK team, we calculate a typical minimum solar viewing time at SOZ of 35 minutes per orbit for at least 85% of the orbits plus 5 minutes for acquisition during the 19° below the xy plane. These calculations account for a 10° unobstructed exclusion window about our line of sight (LOS). Observations begin when the Sun angle reaches the ISS xy plane and continue past the ISS yz plane for a total angle of $\sim 137^\circ$. The β angle is defined as the angle between the orbit plane (ISS xz plane) and the vector from the Sun (e.g., $\beta = 0$ when the Sun is in the ISS xz plane and $+90^\circ$ when it is in the ISS yz plane on the starboard side). For β from 0 to $+40^\circ$ our viewing time is ~ 40 minutes and for 0 to -40° it is ~ 35 minutes due to a truss obstruction on the port side and an ISS module structure to the rear. At β angles of $\pm 55^\circ$, we are limited by solar array obstructions and so there will be no CPI observations at β exceeding these angles. Preliminary review of the JEM site #3 indicates that it is nearly equivalent to SOZ.

5. Mission Overview

5.1. Mission Design

CPI is an Explorer Small Complete Mission intended for the International Space Station (ISS). The baseline ISS site is the Columbus EPF Starboard Overhead Zenith (SOZ) site, and the alternate site is JEM-EF EFU #3. CPI utilizes the ISS resources for transport to the site, attachment via the robotic arm, and for ISS provided telemetry links. The nominal launch date is 1 September 2017. On-orbit checkout continues for two months, followed by 24 months of coronal and solar disk observations. CPI will acquire the Sun at the start of orbital day, starting observations after 5 minutes, and continuing them for about 35 minutes or more. The current average orbital altitude is 400 km and is expected to have increased at the time of CPI operations after the NASA Space Transportation System is retired. The Sun trajectory rises rapidly in the sky during orbital day, providing minimal atmospheric absorption during the observation period. It is estimated that ISS will provide 310 days per year with 16 orbits per day and at least 35 minutes of solar observations (not including 5 minutes for Sun acquisition) per orbit. ISS is well suited to solar experiments because the solar panels are normally aimed at the Sun and out of the line of sight of solar-viewing instruments. ISS engineers assure us that the contamination environment meets the stringent requirements of CPI, but precautions must be taken to not point CPI at the ISS surfaces, and to close its aperture door at times of contamination release and the presence of transport vehicles. A three-year extended mission is proposed. The entire SP will be designed to meet ISS hardware disposal requirements.

5.2. Operations, Data Policy, and Data Archiving

The Science Operations Center will be located at the Smithsonian Astrophysical Observatory (SAO). Ground software will be provided by SAO and based on the command software it developed and used for UVCS/SOHO. The command and telemetry link to the ISS will be provided by the ISS Payload Operations Center (POC) at MSFC. The SAO command software will be upgraded to support communication protocols of the MSFC command and telemetry software that is to be provided to SAO.

CPI will follow NASA's Heliophysics Science Data Management Policy guidelines to make the science data publicly available as quickly as possible. Validated science data will be distributed via the Internet directly from SAO and through the Virtual Solar Observatory with assistance from GSFC's SDA. Level 1 data will be distributed within one month of the time when the data are available to SAO. This will ensure wide dissemination of all CPI data products to the science community.

The validated CPI data products—including associated documentation on calibration methods—will be submitted to the appropriate NSSDC archive as they become available. Level 2 data, calibrated with the best and final calibration parameters, will be provided during the last month of the primary mission.

5.3. Guest Investigator Program

The CPI science team will support an active Guest Investigator (GI) Program during both the primary baseline mission and its continuation to the extent desired by NASA/SMD. It is envisioned that an announcement of opportunity will be released shortly after launch that would consider a broad range of guest participation in the CPI Investigation, supported by about 15 grants per year. These programs will be selected via a rigorous NASA peer review process with the goal of broadly complementing the core team science. GIs will be treated exactly as CPI Co-Investigators, including any desired participation in observation planning.

6. The CPI Team, Management, and Costs

6.1. The CPI Team

The CPI Project is a collaborative effort under the direction of John Kohl, the Principal Investigator, involving a core scientific team from SAO, the University of Montana, and the University of New Hampshire. The PI has delegated the authority to manage the CPI project to the Project Manager, Timothy Norton. The Mission Systems Engineer is Peter Daigneau. George Nystrom will lead the project-level reviews team. The industrial partner is L-3 Communications Integrated Optical Systems (L-3 LOS). Paul Cucchiaro will be the Payload Project Manager for L-3 Com, and Mark Schwalm will be the Payload Systems Engineer. L-3 LOS and its collaborating L-3 Com organizations are highly experienced in the development of space instrumentation and ISS systems and integration, with over 30 years of experience and a 100% success rate on 50+ space flight payloads. It has developed and fielded space-based gimbals, pointing mirrors, SiC UV optics, and grating spectrometers, providing high technical readiness levels against the CPI payload needs. L-3 LOS supported important NASA missions, including gimbaled optical systems for *WISE*, *HIRDLS*, *GIFTS*, and *GOES-R ABI*, and SiC optical systems for *MICSAS*, *ALI*, *HIRDLS*, *LORRI*, and *GOES-R ABI*. L-3 IOS will build the CPI Science Payload drawing on its Tinsley Laboratories facility for aspheric optics and L-3 Communications Systems East (L-3 CSE) for interface expertise with the ISS. L-3 CSE was the primary contractor for the ISS communications and telemetry system with over \$600M in contracts. The CPI ICCD detector system will be procured from Mullard Space Science Laboratory, which cooperated in producing the CPI proposal.

The CPI Science Team includes Dan Reisenfeld who will act as Project Scientist and be responsible for scientific oversight of the CPI development, lead the laboratory and in-flight calibration and characterization

effort including scientific performance tests, and participate in the data analysis. Paul Janzen will be the Instrument Scientist and will be responsible for carrying out the optical design and performance evaluation as well as the laboratory and in-flight calibrations and characterizations. Steven Cranmer will act as Mission Scientist for Solar Wind Science and John Raymond will be the Mission Scientist for CME Science. The CPI Core Science Analysis Team will be greatly strengthened by Ben Chandran, Terry Forbes, Alexander Panasyuk, Phil Isenberg, and Aad van Ballegoijen. In addition to data analysis, Alexander Panasyuk will develop the ground software and head the science operations team.

6.2. Technical Readiness Level and Risks

CPI will be built with existing technology that has extensive heritage. It has no medium or high risks. The Technical Readiness Levels (TRLs) of all CPI hardware is at level 9 or higher.

6.3. Technical Reserves, Cost Reserves, and Margin

Due to the substantial resource capabilities of ISS, mass, power, volume, and telemetry reserves are robust with 54% reserves + margin for mass, 376% for power, 1000% for uplink and downlink and a factor of 2 for pointing.

The CPI budget includes seven months of costed schedule reserve in addition to a schedule that provides 48 months from the start of phase B to the nominal launch date. On top of all PI-Mission Costs and encumbered reserves, there are unencumbered reserves of 25% for phases A/B/C/D leaving 5% margin to the Mission Cost Cap. CPI has a robust descope plan with descopes across the project that would save approximately \$4M. The descopes increase risk by removing redundancy and by using a lower TRL command and data handling system, but the science impact is minimal. Phase E would be shortened by 10% and loss in performance of optical reflection and detector efficiency would be accepted. CPI has no foreign collaborations, contributions, or costs. The ICCD detector system arrangement is a procurement, not an international collaboration.

REFERENCES

- Allen, L. A., et al. 2000, JGR, 105, 23123
Antiochos, S. K., et al. 2011, ApJ, 731, 112
Chandran, B. D. G. 2010, ApJ, 720, 548
Cranmer, S. R. 2009, Living Rev. Sol. Phys., 6, 3
Cranmer, S. R., et al. 1999, ApJ, 511, 481
Cranmer, S. R., et al. 2007, ApJS, 171, 520
Cranmer, S. R., et al. 2008, ApJ, 678, 1480
Cranmer, S. R., et al. 2010, Solar Phys., 263, 275
Cranmer, S. R., & van Ballegoijen, A. A. 2005, ApJS, 156, 265
DeForest, C. E., & Gurman, J. B. 1998, ApJ, 501, L217
De Pontieu, B., et al. 2007, Science, 318, 1574
Esser, R., & Edgar, R. J. 2000, ApJ, 532, L71
Feldman, U., et al. 2007, ApJ, 660, 1674
Fisk, L. A. 2003, JGR, 108, 1157
Frazin, R. A., et al. 2003, ApJ, 597, 1145
Frazin, R. A., et al. 2009, ApJ, 701, 547
Hollweg, J. V., & Isenberg, P. A. 2002, JGR, 107 (A7), 1147

Ko, Y.-K., et al. 2006, ApJ, 646, 1275
Ko, Y.-K., et al. 2010, ApJ, 722, 625
Kohl, J. L., et al. 1978, in *New Instrumentation for Space Astronomy* (Oxford: Pergamon), 91
Kohl, J. L., et al. 1994, *Space Sci. Rev.*, 70, 253
Kohl, J. L., et al. 1995, *Solar Phys.*, 162, 313
Kohl, J. L., et al. 1996, ApJ, 465, L141
Kohl, J. L., et al. 1997, *Solar Phys.*, 175, 613
Kohl, J. L., et al. 1998, ApJ, 501, L127
Kohl, J. L., et al. 1999, ApJ, 510, L59
Kohl, J. L., et al. 2006, *A&A Review*, 13, 31
Kowal, G., et al. 2009, ApJ, 700, 63
Krishna Prasad, S., et al. 2011, *A&A*, 528, L4
Kumar, A., & Rust, D. M. 1996, *JGR*, 101, 15667
Laming, J. M. 2009, ApJ, 695, 954
Landi, E. 2008, ApJ, 685, 1270
Landi, E., et al. 2010, ApJ, 711, 75
Lee, J.-Y., et al. 2009, ApJ, 692, 1271
Lee, L. C., & Wu, B. H. 2000, ApJ, 535, 1014
Lenz, D. D. 2004, ApJ, 604, 433
Lin, J., & Forbes, T. G. 2000, *JGR*, 105, 2375
Lin, J., et al. 2004, ApJ, 602, 422
Lin, R. P., et al. 2010, *Solar Eruptive Events (SEE) 2020 Mission Concept*, white paper submitted to NRC
Solar/Space Physics Decadal Survey
Markovskii, S. A., et al. 2006, ApJ, 639, 1177
Mason, K. O., et al. 2001, *A&A*, 365, L36
Moore, R. L., et al. 2011, ApJ, 731, L18
Murphy, N. A., et al. 2011, ApJ, in press, arXiv:1104.2298
Ofman, L., & Davila, J. M. 2001, ApJ, 553, 935
Panasyuk, A. V. 1999, *JGR*, 104, 9721
Pasachoff, J. M., et al. 2007, ApJ, 665, 824
Raymond, J. C. 2008, *J. Astrophys. Astron.*, 29, 187
Reeves, K. K., et al. 2010, ApJ, 721, 1547
Roming, P. W. A., et al. 2000, *Proc. SPIE*, 4140, 76
Scudder, J. D. 1992, ApJ, 398, 299
Sheeley, N. R., Jr., et al. 1997, ApJ, 484, 472
Sturrock, P. A., & Coppi, B. 1966, ApJ, 143, 3
van der Holst, B., et al. 2010, ApJ, 725, 1373
Viñas, A. F., et al. 2000, ApJ, 528, 509
Voitenko, Y., & Goossens, M. 2004, ApJ, 605, L149
Wilhelm, K. 2006, *A&A*, 455, 697
Withbroe, G. L., et al. 1982, *Space Sci. Rev.*, 33, 17
Yang, S., et al. 2011, ApJ, 732, L7
Yashiro, S., et al. 2004, *JGR*, 109, A07105
Zurbuchen, T. H. 2007, *Ann. Rev. Astron. Astrophys.*, 45, 297